Facultad de Ciencias
Universidad de Cantabria

Search for dark matter production in association with top quarks in the dilepton final state at $\sqrt{s} = 13$ TeV

A thesis submitted in fulfillment of the requirements for the

Degree of Doctor of Philosophy

Written by

Cédric Prieëls

Under the supervision of

Jónatan Piedra Gómez
Pablo Martínez Ruiz del Árbol

Santander, June 2020

Facultad de Ciencias
Universidad de Cantabria

Búsqueda de materia oscura en asociación con quarks top en el estado final dileptónico a $\sqrt{s} = 13$ TeV

Memoria para optar al

Grado de doctor

Escrita por

Cédric Prieëls

Bajo la supervisión de

Jónatan Piedra Gómez
Pablo Martínez Ruiz del Árbol

Santander, Junio 2020

Abstract

Resumen

Acknowledgments

Acronyms used

SM Standard Model

DM Dark Matter

LHC Large Hadron Collider

CMS Compact Muon Solenoid

ATLAS A Toroidal LHC ApparatuS

CERN European Council for Nuclear Research

QFT Quantum Field Theory

CMB Cosmic Microwave Background

ML Machine Learning

MFV Minimal Flavour Violation

WIMP Weakly Interactive Massive Particle

PF Particle Flow

BSM Beyond the Standard Model

MACHO Massive Compact Halo Object

MSSM Minimal Supersymmetric Standard Model

SI Spin Independent

SD Spin Dependent

CL Confidence Level

QCD Quantum ChromoDynamics

ADMX Axion Dark Matter Experiment

CAST CERN Axion Solar Telescope

IAXO International Axion Observatory

LNGS Laboratori Nazionali del Gran Sasso

UED Universal Extra Dimensions

NFW Navarro-Frenk-White

LAT Fermi Large Telescope

IACT Imaging Atmospheric Cherenkov Telescopes

CTA Cherenkov Telescope Array

AMS Alpha Magnetic Spectrometer

EFT Effective Field Theory

ISR Initial State Radiation

FSR Final State Radiation

DMWG Dark Matter Working Group

MET Missing Transverse Energy

VBF Vector Boson Fusion

BR Branching Ratio

LEP Large Electron Positron collider

ALICE A Large Ion Collider Experiment

PS Proton Synchrotron

SPS Super Proton Synchrotron

PU Pile Up

PV Primary Vertex

ECAL Electromagnetic Calorimeter

HCAL Hadronic Calorimeter

DT Drift tube

CSC Cathode Strip Chamber

RPC Resistive Plate Chamber

TIB/TBD Tracker Inner Barrel and Disks

TOB Tracker Outer Barrel

TEC Tracker EndCap

HO Hadron Outer

LS Long Shutdown

GEM Gas Electron Multiplier

L1 Level-1 Trigger

HLT High-Level Trigger

DAQ Data Acquisition System

DQM Data Quality Monitoring

DCS Detector Control System

WP Working Point

SC Super Cluster

KF Kalman Filter

GSF Gaussian Sum Filter

MVA Multi-Variate Analysis

CSV Combined Secondary Vertex

DNN Deep Neural Network

PUPPI Pileup Per Particle Identification

BW Breit-Wigner

MC Monte Carlo

UE Underlying Event

PDF Parton Density Function

LO Leading Order

NLO Next to Leading Order

MPI Multiple Parton Interaction

SF Scale Factors

AOD Analysis Object Data

EDM Event Data Model

DY Drell-Yan

SR Signal Region

CR Control Region

PR Prompt Rate

FR Fake Rate

SS Same Sign

EWK Electroweak

DAS Data Aggregation System

Contents

Chapter 1

Data, signals and backgrounds

In order to find a possible hint of the production of Dark Matter (DM) in the Large Hadron Collider (LHC) collisions considering our signal models of interest, briefly described in Section **??**, the data collected needs to be compared with Monte Carlo (MC) simulations produced in a central way for each Standard Model (SM) process. Indeed, any deviation of the data observed with respect to what we expect to see, obtained from these MC simulations, might be the sign of some Beyond the Standard Model (BSM) physics. All of the steps needed to mathematically simulate the *pp* collisions of the LHC and to take into account the effect of the detector on the particles produced will first of all be introduced in Section 1.1.

Then, the different formats of files available to perform the analysis and the code used will be briefly introduced in Sections 1.2 and 1.3 and the different data samples collected during the Run II of operation of the LHC will be then detailed in Section 1.4, while the signal models and samples considered in this particular analysis along with the MC samples used for the simulation of the different backgrounds will be introduced in Sections 1.5 and 1.6 respectively.

1.1 The Monte Carlo (MC) simulation method

As previously explained, the generation of MC simulations for the most common SM processes is a crucial step of any analysis because they are considered to be the reference to which the data collected is compared in order to try and find some discrepancies, which could the sign of the existence of BSM physics. Searches for exotic physics therefore heavily depend on these simulations, which need to be generated with great care and to which a large uncertainty is typically associated since the collision between the partons of two protons and the interaction between the particles produced and the detector itself are extremely complex by nature.

The basic idea of the MC simulation consists in using a random number generator to simulate the randomness of nature and produce as many events as computationally possible for all the SM processes, taking into account the probability density functions of these processes. This is performed by specific softwares called **event generators** and it is important to note that since we usually don't know everything about the SM or BSM process being generated, the perfect event generator does not exist.

To make the generation of such simulations a bit easier, the description of a typical *pp* collision can usually be divided into several steps that will now be described, as shown with the color code used in Figure 1.1. The typical approximations used to make this kind of simulation possible from the computational point of view will also be briefly introduced at this point.

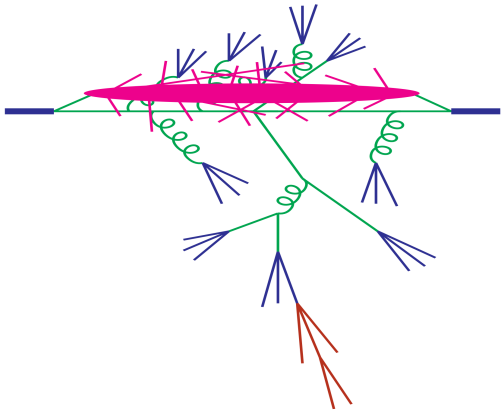

Figure 1.1: Structure of a pp collision and different steps of the MC simulation used by the event generators, such as the parton shower (in green), the Underlying Event (UE) (in pink), the hadronization (in blue) and the decay of unstable particles (in red) [101].

Hard scattering

A typical pp collision at a center of mass energy $\sqrt{s}$ is usually described by an event generator as the interaction between a parton i coming from one proton with a parton j coming from the other, leading to the production of a final state A, made out of n different particles. The total cross section of such process can be expressed with Equation 1.1 [102].

$$\sigma_A(s) = \sum_{i,j} \iint dx1\ dx2\ f_i(x_1, \mu^2)\ f_j(x_2, \mu^2)\ \hat{\sigma}_{ij\to A}(\hat{s}, \mu^2) \tag{1.1}$$

In this equation, several variables have been introduced, such as:

- The artificial parameter μ^2 used as the delimitation between short and long range physics.
- The Parton Density Functions (PDFs) $f_i(x, \mu^2)$ of both partons involved in the collision, giving the probability of finding in the proton a parton of flavor i (quark or gluon) carrying a fraction x of the proton momentum.
- The integrated parton-level cross section $\hat{\sigma}_{ij\to A}$ describing the short range physics between the partons, taking into account the phase space and the matrix element obtained considering all the Feynman diagrams of a given process.
- The square invariant mass of the two partons $\hat{s} = (p_i + p_j)^2$.

Many algorithms have been developed in order to select a hard process $ij \to A$ and determine its kinematics by solving this equation using different methods. The samples used in this work have actually been produced at different orders and by different hard scattering generators, such as MADGRAPH [104] (at LO) and POWHEG [105] and MC@NLO [106] (at NLO).

Parton showers

The parton shower phase is then used to describe what happens to the incoming and outgoing partons after the initial collision that has just been described. The hard process induce by definition

a large acceleration to the partons involved, which then tend to emit Quantum ChromoDynamics (QCD) radiation under the forms of gluons, just like accelerated electric charges do by emitting photons. However, the gluons emitted do have a color charge and can therefore emit further radiation until reaching such a low energy that they are able to form colourless hadrons, as discussed in Section **??**. This process typically leads to the creation of the so-called **parton showers**, approximate higher-order real-emission corrections to the hard scattering, that need to be simulated by the event generators as well since they are an important part of the kinematics of the collision.

The parton showering then consists in simulating these showers for not only the final state particles produced by the hard scattering, but also for the particles in the initial state and for the remnants of the colliding protons, since gluons can actually be emitted by Initial State Radiation (ISR) and by these remnants themselves.

Underlying Event (UE)

Once the hard scattering and all the possible gluon emissions simulated, the next step consists in considering the so-called **Underlying Event (UE)** arising from the parton showers just described and from the secondary collisions between partons not involved in the primary hard process, the so-called Multiple Parton Interactions (MPIs). The UE is usually responsible for the production of particles at low transverse momenta p_T that cannot be experimentally distinguished from particles produced from initial or final state radiation but still need to be simulated.

These secondary collisions typically lead to the production of extra hadrons and therefore need to be simulated as well by events generators, usually by distributing the partons of the incoming protons in an area of 1fm^2: an increased UE will be obtained when the so-called impact parameter, the distance between the parton and the centre of this area, is decreased, making the collision mostly central and almost head-on [107]. The UE is typically well simulated using softwares such as Herwig [108] and PYTHIA [109]. The spectrum for the generation of some variables in a top enriched sample can be found in Figure 1.2.

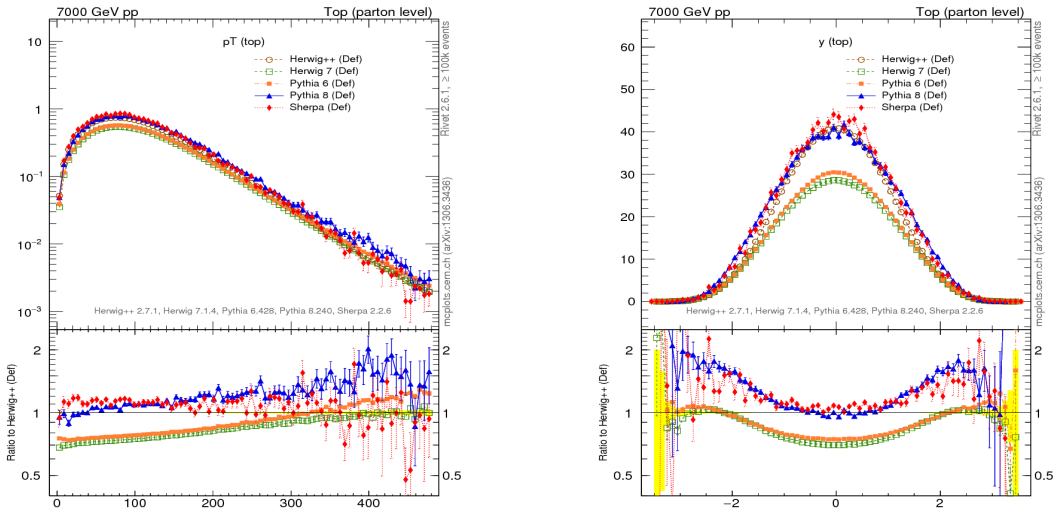

Figure 1.2: Top p_T (on the left) and rapidity (on the right) distributions obtained using different MC generators [110].

Hadronization

Once all the primary and secondary collisions simulated, it is time for the event generators to simulate the **hadronization** and binding processes of the different coloured partons emitted into colourless hadrons, as explained in Section **??**. This hadronization process happen at low energies, when the perturbation theory becomes invalid and the dynamics enter a non-perturbative phase, which leads to the formation of the observed final-state hadrons. Non-perturbative calculations then have to be used by the event generators in order to simulate this effect.

Unstable particle decays

The last step of the MC generation consists in finding a model allowing the unstable hadrons created in the hadronization process to decay, and to study these decays. This is extremely important because experimental data clearly shows that a large fraction of the observed final state particles come from the decays of such excited hadronic states.

Detector simulation

Once the event completely simulated using the event generators and the Pile Up (PU) taken into account by reproducing the hard scattering process several times, another step is required: simulating the interaction between the "perfect" particles previously created and the "imperfect" Compact Muon Solenoid (CMS) detector.

This is typically done by the GEANT4 software [111], able to model different effects, such as:

- Modeling of the interaction region
- Modeling of the particle passage through the volumes that compose CMS detector and of the accompanying physics processes
- Modeling of the effect of multiple interactions per beam crossing and/or the effect of events overlay (PU simulation)
- Modeling of the detector's electronics response

This modeling accounts for all the cracks and for the disposition of the subsystems inside of the CMS detector. This software is for example able to model the interaction of the electrons with the tracker, responsible for the emission of bremsstrahlung photons, as explained in Section **??**.

The results of the comparison between the output of two different versions of the GEANT4 software and prototypes of the CMS calorimeter in the test beam facility at European Council for Nuclear Research (CERN) lead to comparable results, as shown in Figure 1.3.

However, the modeling of the detector is not perfect and not all the inefficiencies can be accounted for. In some cases, Scale Factors (SF) are then used to correct the MC simulations and correct some expected discrepancies between data and MC. This will be detailed later on.

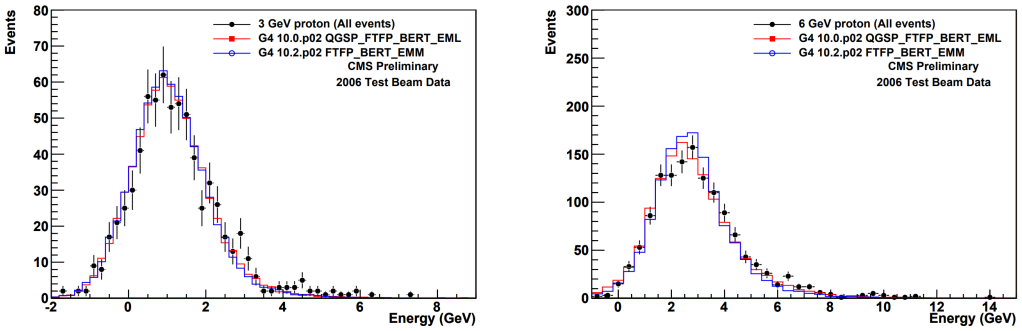

Figure 1.3: Proton energy distribution at 3 (on the left) and 6 (on the right) GeV compared for the test beam data (in black) and two different GEANT4 versions [112].

1.2 Files format

Once recorded (or simulated), the data (or MC) still needs to go under a complete post-processing in order to change its format and reduce the total size of the samples to be considered in the analyses. Different types of analysis are expected to need different levels of data reduction, so the data is usually accessible at different levels [113]:

- Virgin-RAW: used only in low rate runs with heavy ions collisions (10-15Mb/event)
- RAW : standard raw data event content (1Mb/event)
- RECO: detailed information on reconstructed physics objects (3Mb/event)
- Analysis Object Data (AOD): physics objects used in analysis (400-500kB/event)

Two additional formats were introduced since the end of the Run I. First of all the MiniAOD was introduced to reduce the size of the AOD by a factor 10 while retaining most of the information about all the particles that were created, without applying any further selection.

Because of the increased integrated luminosity collected by CMS over the last few years, a brand new file format featuring another reduction of the file size of a factor ~ 50 was recently introduced: the nanoAOD, able to retain most of the information of each collision in around 1kB of data per event only. This reduction in size was achieved by optimizing the floating point of the variables, by not storing quantities that can be recomputed from the available information and by limiting the number of physics objects available, for example. This means that some low-level analyses cannot use this format to work, but it has been estimated that around 50-70% of the analyses performed at CMS can rely on such files in order to work.

In this particular case, the 6th version of the nanoAOD, introducing a series of bug fixes and the latest jet energy corrections, was used for both the data and the MC samples (signal and backgrounds) that will now be listed in the next sections.

1.3 Analysis code

The code used for the event generation, simulation and reconstruction is the version 10_2_X of the official software of the CMS collaboration, called CMSSW [115]. This software contains the CMS Event Data Model (EDM) which is able to describe every event as a C++ object containing all the RAW and reconstructed information related to the collision. These object are stored using the ROOT file format [116], an analysis package writen in C++.

Once all the different samples produced centrally up to the nanoAOD stage, another framework was put in place in order to do a post-processing of such samples, by selecting objects interesting for different dileptonic analyses, reducing therefore even more the size of the samples to be considered by selecting only events having 2 tight leptons. This selection will be detailed in Chapter 2. This *Latino* framework, written in phyton, is common to several different analyses and has been developed by tens of different people over the past few years, providing several tools to produce samples, read the files, apply different corrections to the MC samples and produce the histograms needed to perform a search such as this one.

1.4 Data samples

As already explained in Section **??**, the data analyzed in this work has been taken at a center of mass energy of 13 TeV during the second part of the Run II of operation of the LHC.

During this period, an integrated luminosity of 35.9 ± 0.9 fb^{-1} (2016) [117], 41.5 ± 1.0 fb^{-1} (2017) [118] and 59.7 ± 1.5 fb^{-1} (2018) [119] has been collected, resulting in a total dataset of 137.1 ± 2.0 fb^{-1} recorded by the CMS detector and ready to be analyzed. This data has been obtained by combining a set of single and double lepton triggers that will be described in Section 2.1.1 by taking care of avoiding any eventual double counting due to events present in different triggers. All the data samples considered for this analysis are listed in Section A.1.

1.5 Signal samples

To be completed once the files are actually available Listed in Section A.2.

1.6 Backgrounds prediction

Several different SM background processes have been considered for this analysis, all listed in Section A.3 and mostly estimated directly from MC. In this section, the main backgrounds to consider for this particular analysis will be reviewed, such as:

- The major background for the $t\bar{t}$+DM analysis, the SM $t\bar{t}$, kinematically really close to the signal searched for (Section 1.6.1).
- On the other hand, the major background for the $t/\bar{t}$+DM analysis is the single top production, which has an even higher cross section than the $t\bar{t}$ (Section 1.6.1).

- Then, mainly because of its huge cross section at 13 TeV, as shown in Figure 1.4, the Drell-Yan (DY) process is usually important ton consider. Even though quite reduced in the Signal Regions (SRs) because of the cuts applied, a specific CR will be dedicated to check this background, taken directly from MC (Section 1.6.2).
- The $t\bar{t}+V$ ($t\bar{t}+Z$ and $t\bar{t}+W$) may have a kinematics even closer to our $t\bar{t}$+DM signal than the $t\bar{t}$ process and is therefore extremely important in our signal regions, even though its low cross section does limit its impact (Section 1.6.3).
- Finally, the non-prompt background is another important piece of this analysis mainly because of the particular data-driven method used to compute them (Section 1.6.4).

Add percentage of each background once known

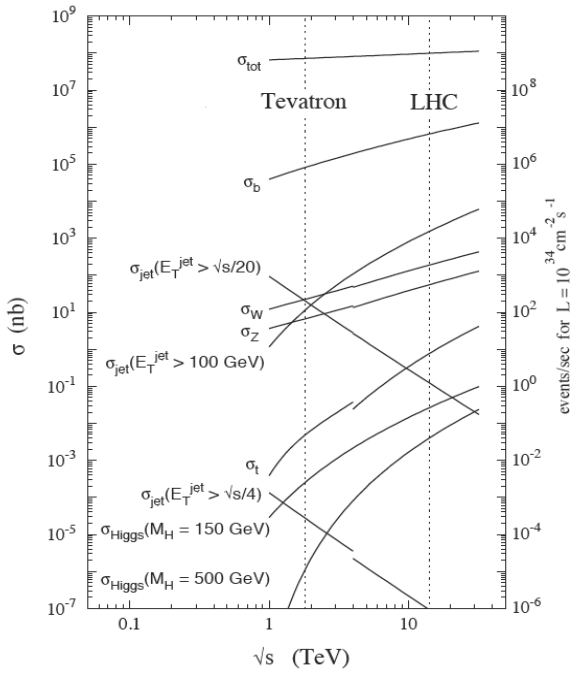

Figure 1.4: Production cross section of the most common SM processes considering different center of mass energies, such as the 13 TeV of the LHC.

Finally, some smaller backgrounds will be introduced in Section 1.6.5, such as the diboson and triboson production, and the weights and corrections applied to all these MC samples will be detailed in Section **??**.

1.6.1 Top production

Because of the relatively high production cross section of top quarks at 13 TeV, the production of a single or a pair of top quarks, but without the production of associated DM, is obviously the dominant background in both searches.

They also have a kinematics quite close to the one expected for our signal: some additional Missing Transverse Energy (MET) is expected because of the production of a pair of DM particles, which might lead to a distribution ϕ distribution as well, but other than that achieving some

discrimination between these processes is quite complex. This process mostly relies on the use of Machine Learning (ML) techniques and will be fully detailed in Section 2.4.

Typically, given the importance of such processes, a specific CR to check for the validity of the CR of such processes is defined, as explained in Section 2.3.

The main background: $t\bar{t}$

Different Feynman diagrams contribute to this process at Leading Order (LO) in a hadron collider, as shown in Figure 1.5. This background is estimated directly from MC and, due to its importance, dedicated CRs have been designed in which to check for the data/MC agreement.

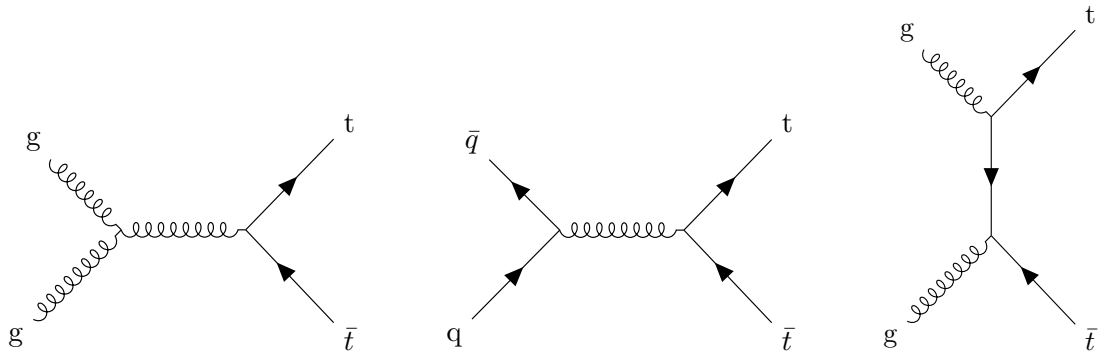

Figure 1.5: Main feynman diagrams for the production of the SM $t\bar{t}$ process.

Single top

Different Feynman diagrams also account for this process in the s-channel (Figure 1.6), t-channel and tW production mode (Figure 1.7).

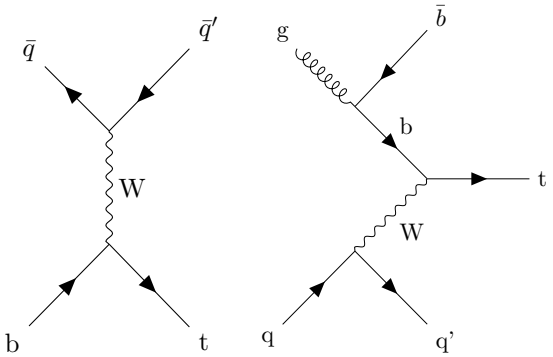

Figure 1.6: Feynman diagrams for s-channel production mode of a single top quarks.

Top decay

As previously mentioned, the top is the heaviest particle of the SM and is expected to decay inside of the beam pipe itself, usually into a bottom quark, giving us a b-jet, and a W boson; this boson can decay itself into different channels even though only its leptonic decay is consider in this particular case. The decay considered of the top/antitop produced is represented in Figure 1.8.

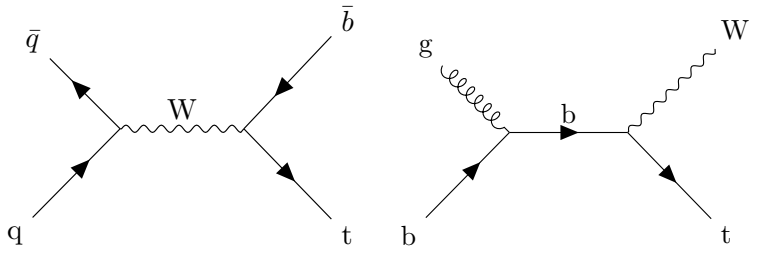

Figure 1.7: Feynman diagrams for t-channel (on the left) and tW (on the right) production modes of a single top quarks.

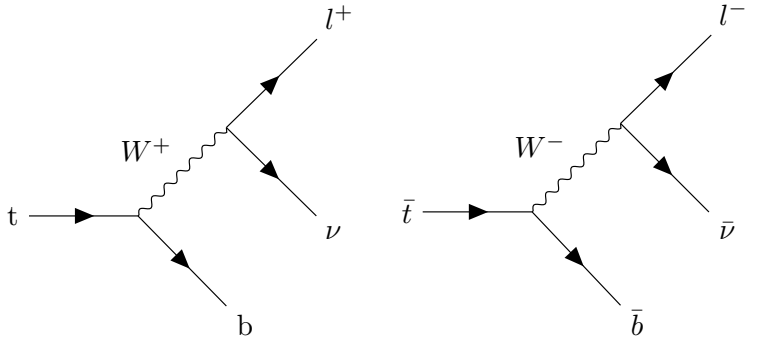

Figure 1.8: Feynman diagrams for the leptonic decay of the top (on the left) and antitop (on the right) quarks.

1.6.2 Drell-Yan estimation

As previously mentioned, most of the DY, produced through the Feynman diagram represented in Figure 1.9, is not expected to survive the selection applied to the analysis but because of the huge cross section of this process, two to three orders of magnitude larger than the production of top, the contribution of this process in the SRs is still quite important.

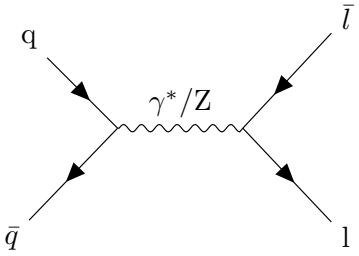

Figure 1.9: Feynman diagram for the DY process involving a virtual γ^* or Z boson.

This background is also estimated from MC as well and is being checked in a specific CR.

1.6.3 $t\bar{t} + V$

This background is coming from a usual $t\bar{t}$ production along with an ISR or Final State Radiation (FSR) production of a W or Z boson, as shown in Figure 1.10. The contribution of this background is also taken directly from MC.

The resulting cross section of such process is a bit lower than the production of the SM $t\bar{t}$ on its

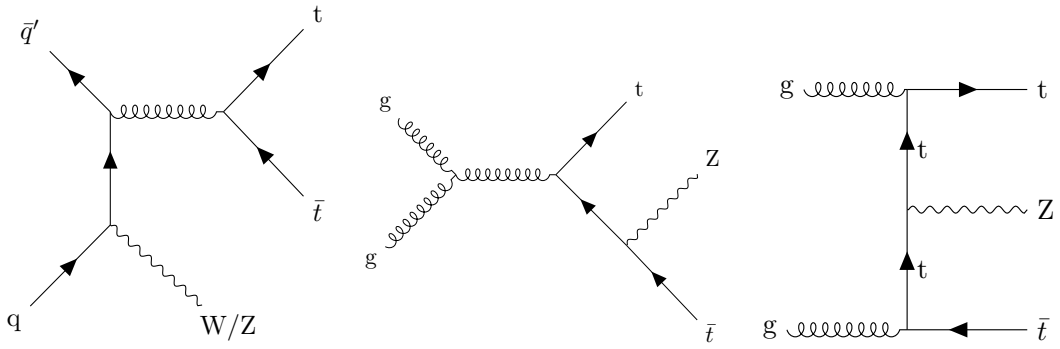

Figure 1.10: Possible Feynman diagrams for the Initial State Radiation (ISR) $t\bar{t}$ with a W/Z boson (on the left) and for the production of an Final State Radiation (FSR) ttZ (on the center and right).

own but the kinematics of this background can be extremely close to our signal, since the W or Z boson produced can give a SM neutrino, leading to some actual MET.

1.6.4 Non prompt contamination

Even though not extremely important in the sense that its kinematics allow us to remove most of its contributions in the SRs, this background is interesting in the sense that is can be estimated using a data-driven method that will now be described instead of being taken directly from MC.

A few definitions are first of all needed to explain the method used to compute the importance of this background in the different regions of the analysis:

- First of all, a **prompt lepton** is defined as a real lepton, in the sense that the lepton is originating from the Primary Vertex (PV) of a *pp* collision.
- The **Prompt Rate (PR)** is defined as the number of prompt leptons passing the tight selection criteria of the analysis over the number of leptons passing the loose selection criteria.
- On the other hand, by **fake** or **non-prompt lepton**, we usually refer to truly **fake leptons**, such as jets misidentified by the detector as leptons, as shown in Figure 1.11, and real leptons coming from eventual heavy flavor decays.
- The **Fake Rate (FR)** is then defined similarly to the prompt rate but considering this time fake leptons only for the tight-to-loose ratio. This ratio therefore corresponds to the probability for a fake lepton to be considered as a real lepton in the analysis.

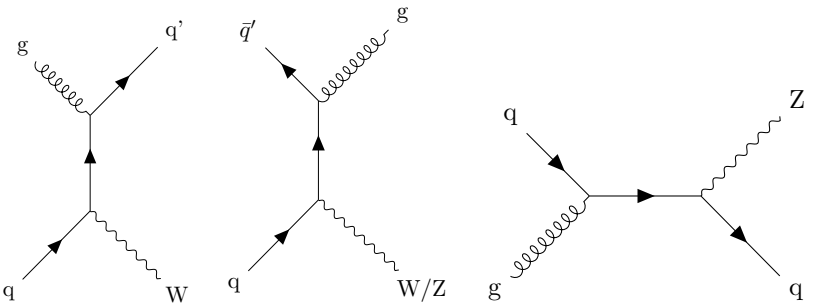

Figure 1.11: Possible Feynman diagrams for the production of a W/Z boson with a jet.

This background is particularly important at low p_T, where the misidentification rate is higher, and is not expected to be modeled correctly by MC because of its complexity: a general **tight-to-loose datadriven method** is then used to compute its kinematics and final contribution in the different regions of the analysis.

In general, this method contains three main steps: the computation of the FR and PR, the extension of these rates in a region kinematically close to the SR of the analysis and the definition of a SS CR enriched in fakes in order to perform a closure test of the yields and kinematics of this background. All these steps will now be detailed.

Fake Rate (FR) computation

Because of its definition, the FR is computed in a prompt lepton-free region, typically in a l1loose QCD enriched region, defined with the following cuts:

- Exactly 1 lepton
- $p_T > 13$ (10) GeV for e (μ)
- $|\eta| < 2.5$ (2.4) for e (μ)
- mtw1 < 20 GeV
- PuppiMET < 20 GeV
- PassJets

All the previous cuts have been designed to define a l1loose QCD region as pure as possible by removing most of the W+jets and Z+jets contribution. The PassJets cut is a boolean obtained by looping over all the jets of the event trying to find a jet having an E_T higher than a given threshold in order to control the average p_T of the jet that fakes the lepton (actually, different FR have been computed for different E_T thresholds, from 10 to 50 GeV).

Using this method, the jet that fakes a lepton is actually the one recoiling against ($\Delta R > 1.0$) the jet used for the systematics, as shown in Figure 1.12.

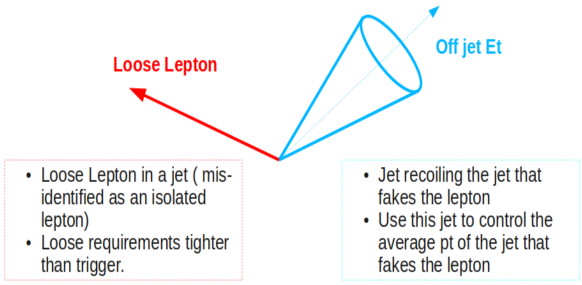

Figure 1.12: Schematic representation of the two jets used for the systematics and for the jet faking a lepton in the tight-to-loose datadriven method.

Events passing the following prescaled triggers are then selected in this region:

$$\text{Muon triggers} = \begin{cases} \text{HLT\_Mu8\_TrkIsoVVL (if } p_T < 20 \text{ GeV)} \\ \text{HLT\_Mu17\_TrkIsoVVL (if } p_T \geq 20 \text{ GeV)} \end{cases} \tag{1.2a}$$

$$\text{Electron triggers} = \begin{cases} \text{HLT\_Ele8\_CaloIdL\_TrackIdL\_IsoVL\_PFJet30 (if } p_T < 25 \text{ GeV)} \\ \text{HLT\_Ele23\_CaloIdL\_TrackIdL\_IsoVL\_PFJet30 (if } p_T \geq 25 \text{ GeV)} \end{cases} \tag{1.2b}$$

The remaining of the Electroweak (EWK) processes (W+jets, Z+jets) able to pass the previous cuts of the QCD region, are then simply substracted: this is the so-called **EWK substraction**.

Since both the FR and PR heavily depend on the kinematics of the event and on the Working Point (WP) chosen for the leptons of the analysis, they are computed separately depending on the flavor of the lepton and 2D histograms (accounting for the p_T and η of the event) need to be created at this stage to calculate this factor, for a given input jet E_T threshold; 1D histograms corresponding to the projections of these 2D histograms along both their axes are also defined at this point, as shown in Figure 1.13.

Prompt Rate (PR) computation

The PR, taking into account the real lepton contamination in the CR defined, is also important to calculate, even though the objects WP are usually chosen is such a way that this ratio is quite close to 1 and can therefore be ignored.

In our case, this rate has been calculated as well using a general tag and probe method in a Z+jets enriched sample. The main objective is to reconstruct $Z \to ll$ events in this region and to select all the events for which the first lepton can be characterized as tight. Then, we search for the second lepton coming from the decay of Z within all the leptons detected by calculating the reconstructed mass of all the possible leptons combinations and selecting the one which is closer to the expected mass of the Z boson. We can then simply count how many times this second lepton, expected to be tight, has actually been measured as a tight lepton to estimate this PR.

The results obtained in this case have been represented in Figure 1.14

Fake weight calculation

Once the fake and prompt rates computed in their specific region, it is still necessary to apply them to a fake-lepton region kinematically close to the SRs of the analysis (usally, a l2loose region). For this, a simple set of equations can be used. We start by defining the following quantities:

- N_{pp} events where both leptons are prompt
- N_{fp} events where one lepton is prompt and the other is fake
- N_{ff} events where both leptons are fake
- N_{tx} $(x = 0, 1, 2)$ events with 0, 1 or 2 leptons passing the right cuts, the **only quantity directly measurable** by the detector

It is then possible to see in Equation 1.3 that, if p is the PR and f the FR previously calculated.

$$\begin{cases} N_l = N_{pp} + N_{fp} + N_{ff} = N_{t2} + N_{t1} + N_{t0} \\ N_{t0} = (1-p)^2 N_{pp} + (1-p)(1-f) N_{fp} + (1-f)^2 N_{ff} \\ N_{t1} = 2p(1-p) N_{pp} + \big(f(1-p) + p(1-f)\big) N_{fp} + 2f(1-f)^2 N_{ff} \\ N_{t2} = p^2 N_{pp} + pf N_{fp} + f^2 N_{ff} \end{cases} \tag{1.3}$$

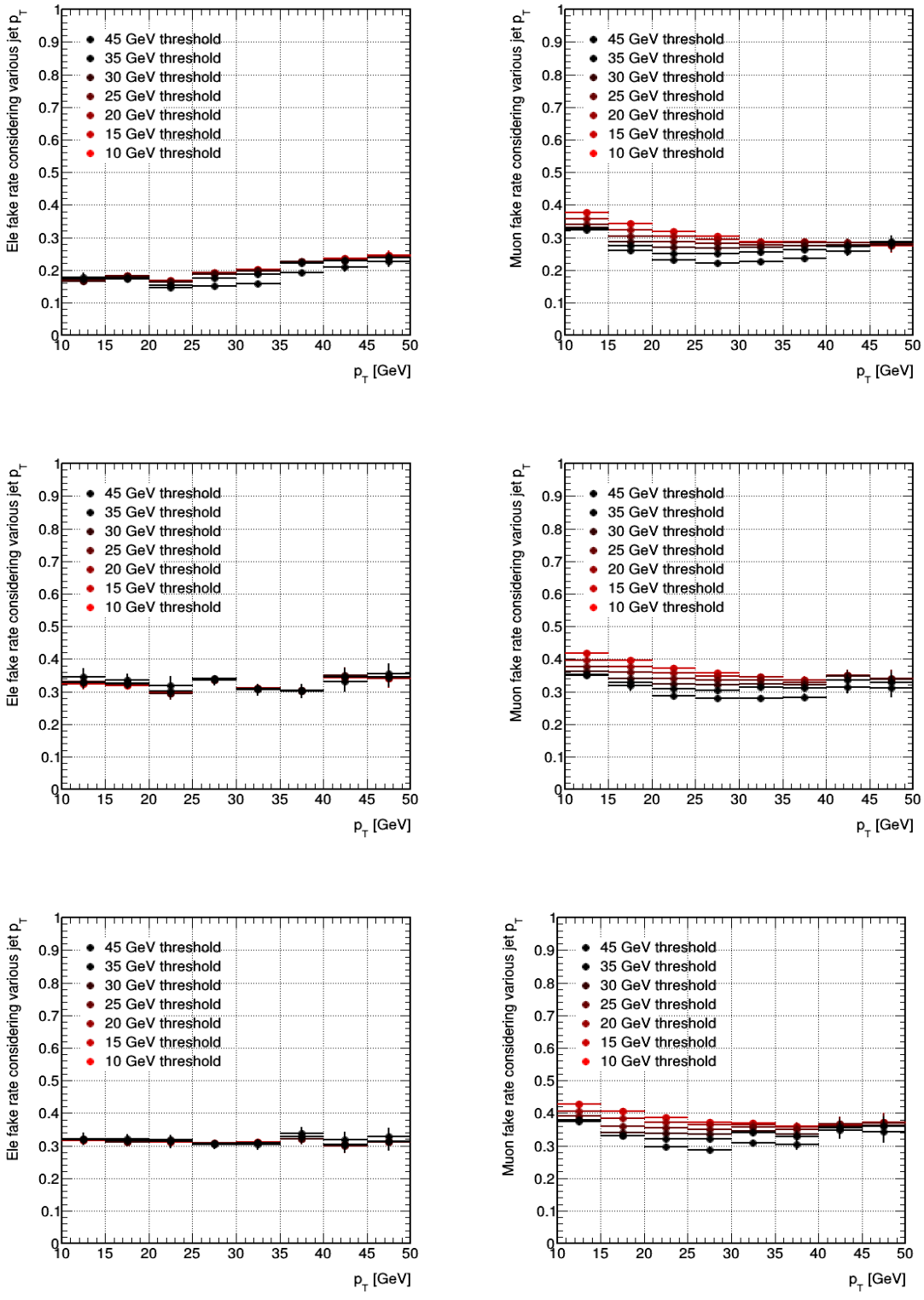

Figure 1.13: Electron (on the left) and muon (on the right) FR obtained in a QCD enriched region for different jet E_T thresholds for 2016 (on the top), 2017 (on the middle) and 2018 (on the bottom) with respect to the p_T of the lepton.

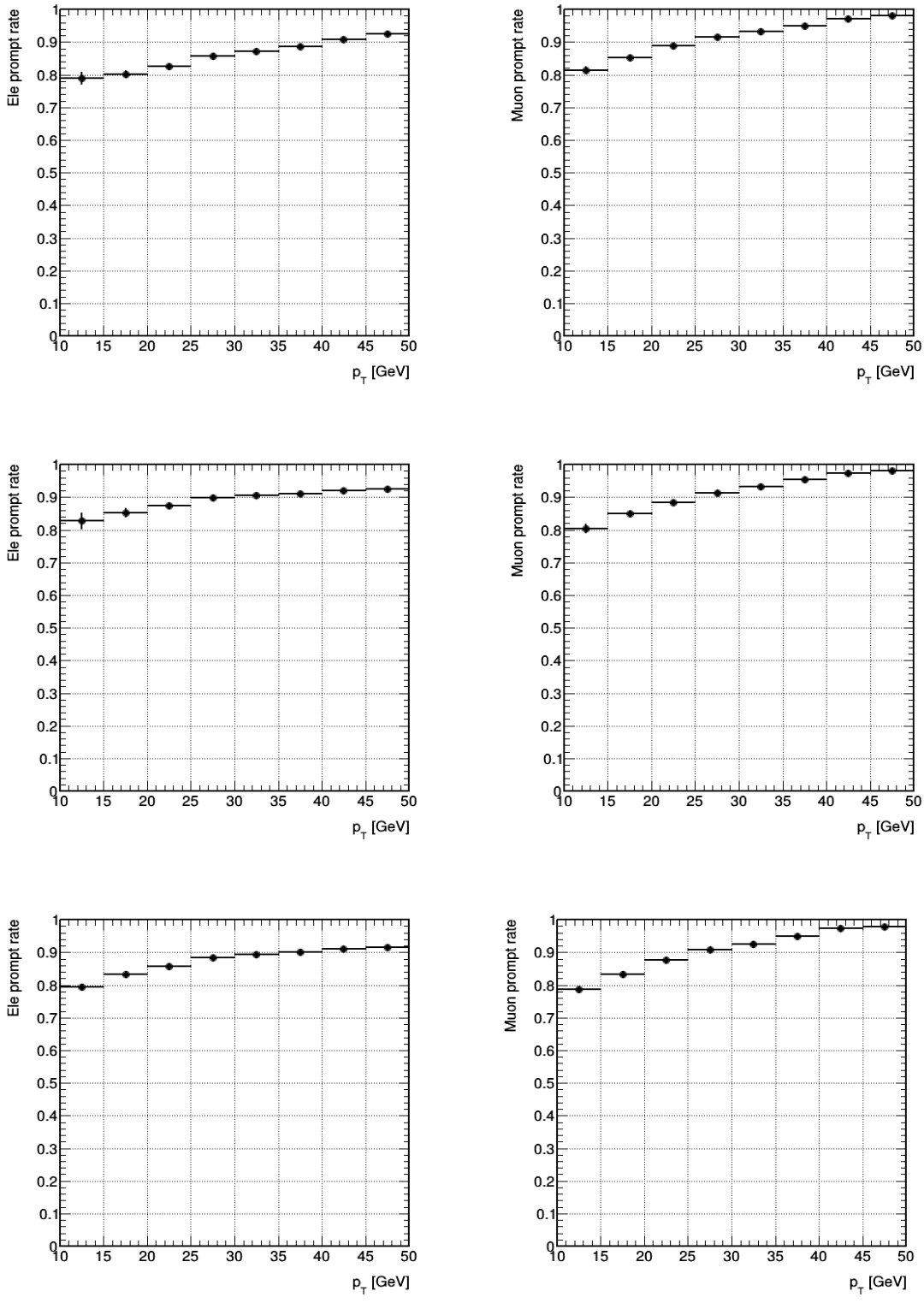

Figure 1.14: Electron (on the left) and muon (on the right) PR obtained in a Z+jets enriched region by a general tag and probe method for 2016 (on the top), 2017 (on the middle) and 2018 (on the bottom) with respect to the p_T of the lepton.

These equations can be inverted in order to represent the unknowns with respect to the known variables, as shown in Equation 1.4, giving us a way to apply the weights previously calculated to this particular l2loose region.

$$\begin{pmatrix} N_{pp} \\ N_{fp} \\ N_{ff} \end{pmatrix} = \frac{f-p}{-(p-f)^3} \cdot \begin{pmatrix} f^2 & -f(1-f) & (1-f)^2 \\ -2fp & p(1-f)+f(1-p) & -2(1-p)(1-f) \\ p^2 & -p(1-p) & (1-p)^2 \end{pmatrix} \cdot \begin{pmatrix} N_{t0} \\ N_{t1} \\ N_{t2} \end{pmatrix} \tag{1.4}$$

Same Sign (SS) control region

Now that we have a way to estimate the kinematics and yields of the non-prompt background in a different region, a Same Sign (SS) CR enriched in fakes is usually defined in order to check this background. This will be done and detailed in Section 2.3.1 of this work.

1.6.5 Smaller backgrounds

Even though quite negligible, some additional backgrounds still need to be considered, such as the dibosons (WW, WZ and ZZ) and tribosons (WWW, WWZ, WZZ, ZZZ) productions, as shown in Figure 1.15. Backgrounds such as the Wγ and Higgs related productions are also considered at this stage. All these smaller backgrounds are taken directly from MC.

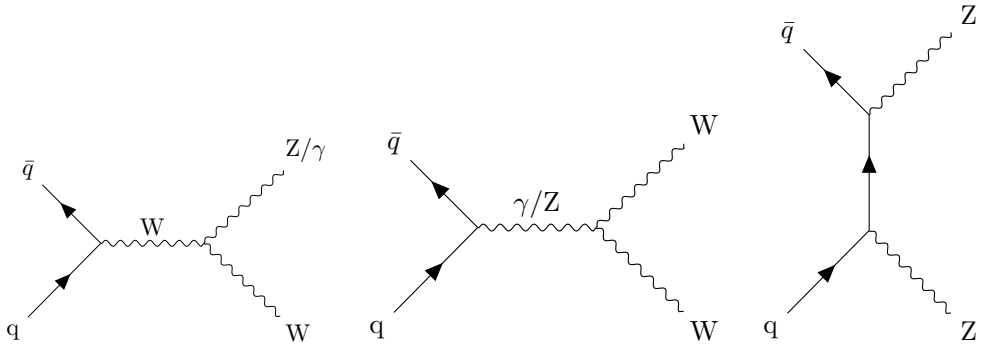

Figure 1.15: Possible Feynman diagrams for smaller backgrounds of this analysis: WW (on the left), Wγ and WZ (on the center) and ZZ (on the right).

Chapter 2

Event selection

This Chapter will be dedicated to the analysis itself, by defining first of all the different objects actually used in this case, along with the actual selection that has been applied to enhance the quality of such objects in this particular search in Section 2.1. Then, the different Signal Regions (SRs) defined in which a high purity of signal is expected are defined in Section 2.2 while all the different Control Regions (CRs) defined in order to check the behavior of the MC simulation performed for the major backgrounds on this analysis, such as the single top or SM $t\bar{t}$ production, will be introduced in Section 2.3.

Finally will come a description about the different variables expected to naturally introduce some discrimination of the $t/\bar{t}$ and $t\bar{t}$+DM signals with respect to the different backgrounds in Section 2.4, along with a global description of the Machine Learning (ML) techniques employed in order to optimize the discriminating power of these variables in the best way possible.

2.1 Objects selection

We already described what to expect from a typical $t/\bar{t}$ or $t\bar{t}$+DM signal: the typical signature of such signals is made out of a certain number of b tagged jets along with two leptons (electrons and/or muons) and some Missing Transverse Energy (MET) coming from the two DM particles created along the way. It is therefore extremely important to describe the Working Point (WP) chosen and the selection applied in order to select the objects of the analysis, such as the leptons and the jets used, in such a way to optimize the lepton reconstruction efficiency while reducing as much as possible the possible misidentification rates of such objects.

First of all, the different triggers used to collect the data will be detailed in Section 2.1.1. Then, the leptons used in this analysis will be introduced in Sections 2.1.2 (for electrons) and 2.1.3 (for muons). Finally, given the nature of the DM signal searched for, a complete description of the jets selected in the analysis will be necessary and performed in Section 2.1.4.

2.1.1 Triggers selection

The triggers, described in Section **??**, and particularly the trigger paths chosen are an important part of each analysis since they will describe the kind of data that can be collected and therefore analyzed. The triggers used in this analysis for the years 2016, 2017 and 2018 can be found in Tables 2.1, 2.2 and 2.1 respectively.

Dataset	Run range	**High-Level Trigger (HLT) trigger path**
SingleMu	[273158,284044]	HLT_IsoMu24_v*
		HLT_IsoTkMu24_v*
SingleEle	[273158,284044]	HLT_Ele27_WPTight_Gsf_v*
		HLT_Ele25_eta2p1_WPTight_Gsf_v*
DoubleEG	[273158,284044]	HLT_Ele23_Ele12_CaloIdL_TrackIdL_IsoVL_DZ_v*
DoubleMu	[273158,281612]	HLT_Mu17_TrkIsoVVL_Mu8_TrkIsoVVL_v*
		HLT_Mu17_TrkIsoVVL_TkMu8_TrkIsoVVL_v*
	[281613,284044]	HLT_Mu17_TrkIsoVVL_Mu8_TrkIsoVVL_DZ_v*
		HLT_Mu17_TrkIsoVVL_TkMu8_TrkIsoVVL_DZ_v*
MuonEG	[273158,278272]	HLT_Mu8_TrkIsoVVL_Ele23_CaloIdL_TrackIdL_IsoVL
		HLT_Mu23_TrkIsoVVL_Ele12_CaloIdL_TrackIdL_IsoVL
	[278273,284044]	HLT_Mu8_TrkIsoVVL_Ele23_CaloIdL_TrackIdL_IsoVL_DZ_v*
		HLT_Mu23_TrkIsoVVL_Ele12_CaloIdL_TrackIdL_IsoVL_DZ_v*

Table 2.1: 2016 trigger paths considered for this analysis.

Dataset	Run range	**HLT trigger path**
SingleMu	[297046,306462]	HLT_IsoMu27_v*
EGamma	[297046,306462]	HLT_Ele35_WPTight_Gsf_v*
		HLT_Ele23_Ele12_CaloIdL_TrackIdL_IsoVL_v*
DoubleMu	[297046,299329]	HLT_Mu17_TrkIsoVVL_Mu8_TrkIsoVVL_DZ_v*
	[299368,306462]	HLT_Mu17_TrkIsoVVL_Mu8_TrkIsoVVL_DZ_Mass8_v*
MuonEG	[297046,306462]	HLT_Mu12_TrkIsoVVL_Ele23_CaloIdL_TrackIdL_IsoVL_DZ_v*
	[297046,299329]	HLT_Mu23_TrkIsoVVL_Ele12_CaloIdL_TrackIdL_IsoVL_DZ_v*
	[299368,306462]	HLT_Mu23_TrkIsoVVL_Ele12_CaloIdL_TrackIdL_IsoVL_v*

Table 2.2: 2017 trigger paths considered for this analysis.

Dataset	Run range	**HLT trigger path**
SingleMu	[315252,325172]	HLT_IsoMu24_v*
		HLT_Mu5_v*
	[314859,325175]	HLT_IsoMu27_v*
EGamma	[315252,325172]	HLT_Ele32_WPTight_Gsf_v*
		HLT_Ele35_WPTight_Gsf_v*
		HLT_Ele23_Ele12_CaloIdL_TrackIdL_IsoVL_v*
DoubleMu	[315252,325172]	HLT_Mu17_TrkIsoVVL_Mu8_TrkIsoVVL_DZ_Mass3p8_v*
		HLT_Mu17_TrkIsoVVL_Mu8_TrkIsoVVL_DZ_Mass8_v*
MuonEG	[315252,325172]	HLT_Mu23_TrkIsoVVL_Ele12_CaloIdL_TrackIdL_IsoVL_v*
		HLT_Mu12_TrkIsoVVL_Ele23_CaloIdL_TrackIdL_IsoVL_DZ_v*

Table 2.3: 2018 trigger paths considered for this analysis.

Our analysis relying on the dilepton final state, the single lepton trigger are only considered in order to recover some of the efficiency lost in some cases when one lepton passes the tight identification criteria while the second one does not, and does therefore not trigger the event. The logical *or* of all the trigger paths are usually considered. Eventual events passing several triggers is taken into account as well to make sure to avoid any double counting due to this effect.

These triggers have been studied in order to make sure that they are efficient enough in the p_T region of the leptons of the analysis to avoid any undesired effect due to the turn-on of any trigger. These trigger efficiencies, calculated using a general tag and probe method and found for example for different runs of the 2017 data taking period in Figure 2.1 for a DoubleEG trigger, are then used to reweight the simulated samples.

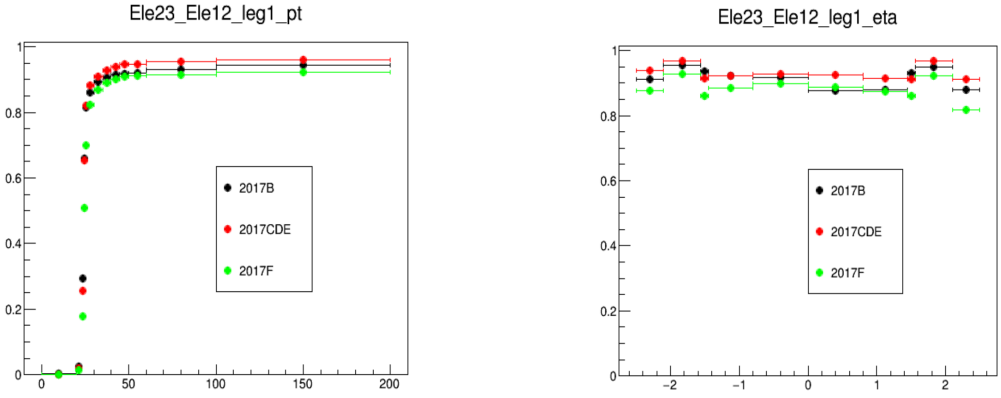

Figure 2.1: DougleEG trigger efficiencies with respect to the p_T (on the left) and η (on the right), computed using a tag and probe method, for the 2017 data taking period.

2.1.2 Electron selection

2.1.3 Muon selection

2.1.4 Jet selection

2.2 Signal regions

It is important to note that a strict **blinding policy** has been followed for this search, in order to avoid optimizing the analysis based on what has already seen. The data available to be ploted in the following signal regions has therefore been limited to 1 fb^{-1} for each year.

2.3 Control regions

2.3.1 Same Sign (SS) CR

2.4 Background-signal discrimination

2.4.1 Discriminating variables

Missing Transverse Energy (MET)

This variable has already been defined in Section **??**, and corresponds to the imbalance in transverse momentum which can be left by different phenomena, such as the apparition of a SM neutrino or the existence of DM particles, able to escape the detector without being detected.

This variable is expected to induce some discrimination between the signal and the backgrounds because, even tough the $t\bar{t}$ in the dilepton final state is expected to produce two neutrinos and therefore some MET, the $t\bar{t}$+DM signal model is expected to have mostly the same contribution to the MET from its own two neutrinos, and an additional contributions from the pair $\chi\bar{\chi}$ produced. The MET spectrum is therefore expected to reach higher values for the signal than the backgrounds.

TALK ABOUT SINGLE TOP?

Stransverse mass

The m_{T2} variable, also called **stransverse mass**, is an extension of the definition of the transverse mass m_T to cases when pairs of particles with the same flavor decay into one visible and one invisible particle, such as what happens in the $W \to l\nu$ decay, for example.

In this particular case, two particles contribute to the presence of Missing Transverse Energy (MET)

and the individual contribution of each particle ($\not{\boldsymbol{p}}_{\boldsymbol{T_1}}$ and $\not{\boldsymbol{p}}_{\boldsymbol{T_2}}$) to this missing energy cannot be inferred. The stransverse mass is then defined according to Equation 2.1, where $\boldsymbol{p}_{\boldsymbol{T_i}} = \overrightarrow{p_{T_i}}$ is the (visible) transverse momentum of the particle i and α is the angle between the visible and invisible p_T of the decay considered [114].

$$\begin{cases} M_{T2}^2 = \min\limits_{\not{\boldsymbol{p}}_{\boldsymbol{T_1}}+\not{\boldsymbol{p}}_{\boldsymbol{T_2}}=\not{\boldsymbol{p}}_{\boldsymbol{T}_{\text{tot}}}} \left(\max \left(m_T^2(\boldsymbol{p}_{\boldsymbol{T_1}}, \not{\boldsymbol{p}}_{\boldsymbol{T_1}}), m_T^2(\boldsymbol{p}_{\boldsymbol{T_2}}, \not{\boldsymbol{p}}_{\boldsymbol{T_2}}) \right) \right) \\ m_T^2(\boldsymbol{p}_{\boldsymbol{T}}, \not{\boldsymbol{p}}_{\boldsymbol{T}}) = 4\ |\boldsymbol{p}_{\boldsymbol{T}}||\not{\boldsymbol{p}}_{\boldsymbol{T}}|\ \sin^2\left(\frac{\alpha}{2}\right) \end{cases} \tag{2.1}$$

This equation can be understood in the following way: to compute the m_{T2} variable, different combinations ($\not{\boldsymbol{p}}_{\boldsymbol{T_1}}$, $\not{\boldsymbol{p}}_{\boldsymbol{T_2}}$) satisfying the condition $\not{\boldsymbol{p}}_{\boldsymbol{T_1}} + \not{\boldsymbol{p}}_{\boldsymbol{T_2}} = \not{\boldsymbol{p}}_{\boldsymbol{T}_{\text{tot}}}$ need to be probed, keeping only the combination which results in the lowest value.

In this particular analysis, $M_{T2}(ll)$ is calculated, since the role of the visible particles is played by the two final state leptons. This variable is expected to introduce some discrimination because, according to the definition just given, the $M_{T2}(ll)$ variable for a SM $t\bar{t}$ process is expected to have an endpoint exactly at the mass of the W boson, while an eventual $t\bar{t}$+DM signal does not have this limitation in the $M_{T2}(ll)$ spectrum because of the pair of DM particles produced, which also contributes to the total MET of the event.

However, in practice, we do observe a tail in this spectrum even for SM $t\bar{t}$ without DM, because of the instrumental MET sometimes observed or the fact that some selected leptons are not actually prompt leptons but can be jets misidentified as leptons by the detector.

TALK ABOUT SINGLE TOP?

2.4.2 Neural network

Chapter 3

Results and interpretations

3.1 Systematics and uncertainties

3.2 Results

Chapter 4

Conclusions

4.1 Future prospects

Appendices

Appendix A

Samples used

A.1 Data samples

All the data samples considered for this analysis are listed in Tables A.1, A.2 and A.3. The luminosity of each dataset has been computed using the Brilcalc tool provided by CMS [120], while the number of generated events has been obtained using the CERN official Data Aggregation System (DAS).

A.2 Signal samples

To be completed once the files are actually available

A.3 Backgrounds samples

To be completed once the analysis actually performed LO/NLO Generator used

Dataset	Events (size)	$\mathcal{L}$ [fb^{-1}]
Run 2016B		
/DoubleEG/Run2016B_ver2-Nano1June2019_ver2-v1/NANOAOD	143073268 (99.4Gb)	
/DoubleMuon/Run2016B_ver2-Nano1June2019_ver2-v1/NANOAOD	82535526 (53.2Gb)	
/MuonEG/Run2016B_ver2-Nano1June2019_ver2-v1/NANOAOD	32727796 (26.8Gb)	5.8
/SingleElectron/Run2016B_ver2-Nano1June2019_ver2-v1/NANOAOD	246440440 (167.8Gb)	
/SingleMuon/Run2016B_ver2-Nano1June2019_ver2-v1/NANOAOD	158145722 (96.4Gb)	
Run 2016C		
/DoubleEG/Run2016C-Nano1June2019-v1/NANOAOD	47677856 (35.3Gb)	
/DoubleMuon/Run2016C-Nano1June2019-v1/NANOAOD	27934629 (19.7Gb)	
/MuonEG/Run2016C-Nano1June2019-v1/NANOAOD	15405678 (12.8Gb)	2.6
/SingleElectron/Run2016C-Nano1June2019-v1/NANOAOD	97259854 (69.3Gb)	
/SingleMuon/Run2016C-Nano1June2019-v1/NANOAOD	67441308 (42.4Gb)	
Run 2016D		
/DoubleEG/Run2016D-Nano1June2019-v1/NANOAOD	53324960 (39.6Gb)	
/DoubleMuon/Run2016D-Nano1June2019-v1/NANOAOD	33861745 (24.1Gb)	
/MuonEG/Run2016D-Nano1June2019-v1/NANOAOD	23482352 (19.4Gb)	4.2
/SingleElectron/Run2016D-Nano1June2019-v1/NANOAOD	148167727 (104.4Gb)	
/SingleMuon/Run2016D-Nano1June2019-v1/NANOAOD	98017996 (61.3Gb)	
Run 2016E		
/DoubleEG/Run2016E-Nano1June2019-v1/NANOAOD	49877710 (37.9Gb)	
/DoubleMuon/Run2016E-Nano1June2019-v1/NANOAOD	28246946 (20.8Gb)	
/MuonEG/Run2016E-Nano1June2019-v2/NANOAOD	22519303 (19.0Gb)	4.0
/SingleElectron/Run2016E-Nano1June2019-v1/NANOAOD	117321545 (86.5Gb)	
/SingleMuon/Run2016E-Nano1June2019-v1/NANOAOD	90984718 (58.7Gb)	
Run 2016F		
/DoubleEG/Run2016F-Nano1June2019-v1/NANOAOD	34577629 (26.9Gb)	
/DoubleMuon/Run2016F-Nano1June2019-v1/NANOAOD	20329921 (15.3Gb)	
/MuonEG/Run2016F-Nano1June2019-v1/NANOAOD	16002165 (13.6Gb)	3.1
/SingleElectron/Run2016F-Nano1June2019-v1/NANOAOD	70593532 (51.4Gb)	
/SingleMuon/Run2016F-Nano1June2019-v1/NANOAOD	65489554 (42.4Gb)	
Run 2016G		
/DoubleEG/Run2016G-Nano1June2019-v1/NANOAOD	78797031 (61.6Gb)	
/DoubleMuon/Run2016G-Nano1June2019-v1/NANOAOD	45235604 (34.2Gb)	
/MuonEG/Run2016G-Nano1June2019-v1/NANOAOD	33854612 (29.0Gb)	7.6
/SingleElectron/Run2016G-Nano1June2019-v1/NANOAOD	153363109 (109.2Gb)	
/SingleMuon/Run2016G-Nano1June2019-v1/NANOAOD	149912248 (94.6Gb)	
Run 2016H		
/DoubleEG/Run2016H-Nano1June2019-v1/NANOAOD	85388734 (67.7Gb)	
/DoubleMuon/Run2016H-Nano1June2019-v1/NANOAOD	48912812 (37.3Gb)	
/MuonEG/Run2016H-Nano1June2019-v1/NANOAOD	29236516 (26.0Gb)	8.6
/SingleElectron/Run2016H-Nano1June2019-v1/NANOAOD	128854598 (93.8Gb)	
/SingleMuon/Run2016H-Nano1June2019-v1/NANOAOD	174035164 (110.2Gb)	

Table A.1: Datasets collected in 2016 and considered for this analysis.

Dataset	Events (size)	$\mathcal{L}$ [fb^{-1}]
Run 2017B		
/DoubleEG/Run2017B-Nano1June2019-v1/NANOAOD	58088760 (46.6Gb)	
/DoubleMuon/Run2017B-Nano1June2019-v1/NANOAOD	14501767 (10.8Gb)	
/SingleElectron/Run2017B-Nano1June2019-v1/NANOAOD	60537490 (42.2Gb)	4.8
/SingleMuon/Run2017B-Nano1June2019-v1/NANOAOD	136300266 (86.2Gb)	
/MuonEG/Run2017B-Nano1June2019-v1/NANOAOD	4453465 (4.1Gb)	
Run 2017C		
/DoubleEG/Run2017C-Nano1June2019-v1/NANOAOD	65181125 (53.8Gb)	
/DoubleMuon/Run2017C-Nano1June2019-v1/NANOAOD	49636525 (39.5Gb)	
/SingleElectron/Run2017C-Nano1June2019-v1/NANOAOD	136637888 (102.5Gb)	9.7
/SingleMuon/Run2017C-Nano1June2019-v1/NANOAOD	165652756 (109.5Gb)	
/MuonEG/Run2017C-Nano1June2019-v1/NANOAOD	15595214 (15.0Gb)	
Run 2017D		
/DoubleEG/Run2017D-Nano1June2019-v1/NANOAOD	25911432 (21.6Gb)	
/DoubleMuon/Run2017D-Nano1June2019-v1/NANOAOD	23075733 (18.6Gb)	
/SingleElectron/Run2017D-Nano1June2019-v1/NANOAOD	51526710 (38.5Gb)	4.2
/SingleMuon/Run2017D-Nano1June2019-v1/NANOAOD	70361660 (47.2Gb)	
/MuonEG/Run2017D-Nano1June2019-v1/NANOAOD	9164365 (8.9Gb)	
Run 2017E		
/DoubleEG/Run2017E-Nano1June2019-v1/NANOAOD	56233597 (49.8Gb)	
/DoubleMuon/Run2017E-Nano1June2019-v1/NANOAOD	51589091 (44.4Gb)	
/SingleElectron/Run2017E-Nano1June2019-v1/NANOAOD	102121689 (81.3Gb)	9.3
/SingleMuon/Run2017E-Nano1June2019-v1/NANOAOD	154630534 (111.0Gb)	
/MuonEG/Run2017E-Nano1June2019-v1/NANOAOD	19043421 (19.2Gb)	
Run 2017F		
/DoubleEG/Run2017F-Nano1June2019-v1/NANOAOD	74307066 (67.1Gb)	
/DoubleMuon/Run2017F-Nano1June2019-v1/NANOAOD	79756560 (68.0Gb)	
/SingleElectron/Run2017F-Nano1June2019-v1/NANOAOD	128467223 (105.2Gb)	13.5
/SingleMuon/Run2017F-Nano1June2019-v1/NANOAOD	242135500 (178.3Gb)	
/MuonEG/Run2017F-Nano1June2019-v1/NANOAOD	25776363 (26.3Gb)	

Table A.2: Datasets collected in 2017 and considered for this analysis.

Dataset	Events (size)	$\mathcal{L}$ [fb^{-1}]
Run 2018A		
/DoubleMuon/Run2018A-Nano25Oct2019-v1/NANOAOD	75499908 (62.6Gb)	13.5
/EGamma/Run2018A-Nano25Oct2019-v1/NANOAOD	327843843 (261.8Gb)	
/SingleMuon/Run2018A-Nano25Oct2019-v1/NANOAOD	241608232 (167.7Gb)	
/MuonEG/Run2018A-Nano25Oct2019-v1/NANOAOD	32958503 (32.3Gb)	
Run 2018B		
/DoubleMuon/Run2018B-Nano25Oct2019-v1/NANOAOD	35057758 (28.3Gb)	6.8
/EGamma/Run2018B-Nano25Oct2019-v1/NANOAOD	153822427 (123.1Gb)	
/SingleMuon/Run2018B-Nano25Oct2019-v1/NANOAOD	119918017 (82.3Gb)	
/MuonEG/Run2018B-Nano25Oct2019-v1/NANOAOD	16211567 (15.8Gb)	
Run 2018C		
/DoubleMuon/Run2018C-Nano25Oct2019-v1/NANOAOD	34565869 (27.6Gb)	6.6
/EGamma/Run2018C-Nano25Oct2019-v1/NANOAOD	147827904 (119.2Gb)	
/SingleMuon/Run2018C-Nano25Oct2019-v1/NANOAOD	110032072 (75.7Gb)	
/MuonEG/Run2018C-Nano25Oct2019-v1/NANOAOD	15652198 (15.3Gb)	
Run 2018D		
/DoubleMuon/Run2018D-Nano25Oct2019_ver2-v1/NANOAOD	168605834 (128.6Gb)	32.0
/EGamma/Run2018D-Nano25Oct2019-v1/NANOAOD	751348648 (583.6Gb)	
/SingleMuon/Run2018D-Nano25Oct2019-v1/NANOAOD	513867253 (344.5Gb)	
/MuonEG/Run2018D-Nano25Oct2019_ver2-v1/NANOAOD	71961587 (68.6Gb)	

Table A.3: Datasets collected in 2018 and considered for this analysis.

List of figures

List of tables

Bibliography

[1] F. Englert and R. Brout, "Broken symmetry and the mass of gauge vector mesons", Phys. Rev. Lett. 13, pp. 321-323, 1964

[2] P. W. Higgs, "Broken symmetries and the masses of gauge bosons", Phys. Rev. Lett. 13, pp. 508-509, 1964

[3] S. Chatrchyan et al., "Observation of a new boson at a mass of 125 GeV with the CMS experiment at the LHC", Phys. Lett. B716, pp. 30-61, 2012 [arXiv: 1207.7235]

[4] G. Aad et al., "Observation of a new particle in the search for the Standard Model Higgs boson with the ATLAS detector at the LHC", Phys. Lett. B716, pp. 1-29, 2012 [arXiv: 1207.7214]

[5] V.C. Rubin, W.K. Ford and N. Thonnard, "Rotational properties of 21 SC galaxies with a large range of luminosities and radii, from NGC 4605 (R=4kpc) to UGC 2885 (R=122kpc)", Astrophysical Journal 238, pp. 471-487, 1980

[6] K.G. Begeman, A.H. Broeils and R.H. Sanders, "Extended rotation curves of spiral galaxies - Dark haloes and modified dynamics", Monthly Notices of the Royal Astronomical Society, vol. 249, issue 3, ISSN 0035-8711, 1991

[7] A. Robertson, R. Massey and V. Eke, "What does the Bullet Cluster tell us about self-interacting dark matter?", Monthly Notices of the Royal Astronomical Society, vol. 465, issue 1, 2017 [arXiv: 1605.04307]

[8] J.B. Mu?oz, C. Dvorkin and A. Loeb, "21-cm Fluctuations from Charged Dark Matter", Phys. Rev. Lett. 121, 121301 (2018) [arXiv: 1804.01092]

[9] A. Natarajan, "A closer look at CMB constraints on WIMP dark matter", Phys. Rev. D85, 2012 [arXiv:1201.3939]

[10] G. D'Ambrosio G.F. Giudice, G. Isidori and A. Strumia, "Minimal Flavour Violation: an effective field theory approach", Nucl.Phys. 645, pp 155-187, 2002 [arXiv:0207.036]

[11] CMS Collaboration, "Search for the production of dark matter in association with top-quark pairs in the single-lepton final state in proton-proton collisions at $\sqrt{s} = 8$ TeV", JHEP, vol. 6 121, 2015

[12] CMS Collaboration,, "Search for the Production of Dark Matter in Association with Top Quark Pairs in the Di-lepton Final State in pp collisions at $\sqrt{s} = 8$ TeV", CMS-PAS-B2G-13-004, 2014

[13] "Search for dark matter in events with heavy quarks and missing transverse momentum in pp collisions with the ATLAS detector", Eur. Phys. J. C (2015) 75:92

[14] ATLAS Collaboration, Search for the Supersymmetric Partner of the Top Quark in the Jets+Emiss Final State at $\sqrt{s} = 13$ TeV", ATLAS-CONF-2016-077

[15] ATLAS Collaboration, "Search for top squarks in final states with one isolated lepton, jets, and missing transverse momentum in $\sqrt{s} = 13$ TeV pp collisions with the ATLAS detector", ATLAS-CONF-2016-050, 2016

[16] ATLAS Collaboration, "Search for direct top squark pair production and dark matter production in final states with two leptons in $\sqrt{s} = 13$ TeV pp collisions using 13.3 fb^{-1} of ATLAS data", ATLAS-CONF-2016-076, 2016

[17] ATLAS Collaboration, "Search for dark matter produced in association with bottom or top quarks in $\sqrt{s} = 13$ TeV pp collisions with the ATLAS detector", Eur. Phys. J. C 78 (2018) 18 [arXiv: 1710.11412]

[18] CMS Collaboration, Search for dark matter produced in association with heavy-flavor quark pairs in proton-proton collisions at $\sqrt{s} = 13$ TeV", Eur. Phys. J. C (2017) 77: 845

[19] CMS Collaboration, "Search for dark matter particles produced in association with a top quark pair at $\sqrt{s} = 13$ TeV", Phys. Rev. Lett. 122, 011803 (2019) [arXiv: 1807.06522]

[20] CMS Collaboration, "Search for dark matter produced in association with a single top quark or a top quark pair in proton-proton collisions at $\sqrt{s} = 13$ TeV", JHEP, vol. 03 141, 2019 [arXiv: 1901.01553]

[21] S. Manzoni, "The Standard Model and the Higgs Boson", Physics with Photons Using the ATLAS Run 2 Data, Springer Theses, 2019

[22] A.B. Balantekin, A. Gouvea and B.Kayser, "Addressing the Majorana vs. Dirac Question with Neutrino Decays", FERMILAB-PUB-18-418-T, NUHEP-TH/18-09 [arXiv: 1808.10518]

[23] J. Woithe, G.J. Wiener and F. Van der Vecken, "Let's have a coffee with the Standard Model of particle physics!", Physics education 52, number 3, 2017

[24] F. Zwicky, "Die Rotverschiebung von extragalaktischen Nebeln", Helvetica Physica Acta , vol. 6, pp. 110-127, 1933

[25] S. Van den Bergh,Phys Rev D "The early history of dark matter", Dominion Astrophysical Observatory, 1999

[26] V.C. Rubin, W.K. Ford, "Rotation of the Andromeda Nebula from a Spectroscopic Survey of Emission Regions", Astrophysical Journal 159, p. 379, 1970

[27] A. A. Penzias, R.W. Wilson, "A Measurement of Excess Antenna Temperature at 4080 Mc/s", Astrophysical Journal 142, pp. 419-421

[28] D.J. Fixsen, "The temperature of the cosmic microwave background", Astrophysical Journal, 2009

[29] Planck Collaboration, "Planck 2018 results. I. Overview and the cosmological legacy of Planck", 2018 [arXiv: 1807.06205]

[30] R. Tojeiro, "Understanding the Cosmic Microwave Background Temperature Power Spectrum", 2006

[31] Planck Collaboration, "Planck 2018 results. VI. Cosmological parameters", 2018 [arXiv: 1807.06209]

[32] "Astrophysical Constants and Parameters", 2019

[33] D. Clowe et all., "A Direct Empirical Proof of the Existence of Dark Matter", Astrophysical Journal Letters 648, 2006

[34] K.R. Dienes, J. Fennick, J. Kumar, B. Thomas "Dynamical Dark Matter from Thermal Freeze-Out", Phys. Rev. D 97, 063522 (2018) [arXiv: 1712.09919]

[35] C.S. Frenk, S.D.M. White, "Dark matter and cosmic structure", Annalen der Physik, p. 22 , 2012 [arXiv: 1210.0544]

[36] R. Kirk, "Dark matter genesis"

[37] M. Drewes et all., "A White Paper on keV Sterile Neutrino Dark Matter", 2016 [arXiv: 1602.04816]

[38] C. Alcock et all., "The MACHO Project: Microlensing Results from 5.7 Years of LMC Observations", Astrophys.J. 542 (2000) 281-307

[39] P. Tisserand et all., "Limits on the Macho content of the Galactic Halo from the EROS-2 Survey of the Magellanic Clouds", A & A 469, pp. 387-404 (2007)

[40] EROS and MACHO collaborations, "EROS and MACHO Combined Limits on Planetary Mass Dark Matter in the Galactic Halo", 1998

[41] Particle Data Group, "Neutrino Cross Section Measurements", PDG 2019

[42] K. McFarland, "Neutrino Interactions", 2008 [arXiv: 0804.3899]

[43] E. Morgante, "Aspects of WIMP Dark Matter Searches at Colliders and Other Probes", Springer theses, 2016

[44] F. Couchot et all., "Cosmological constraints on the neutrino mass including systematic uncertainties", A & A 606, A104 (2017)

[45] E. Bulbul et all., "Detection of An Unidentified Emission Line in the Stacked X-ray spectrum of Galaxy Clusters", 2014 [arXiv: 1402.2301]

[46] A. Boyarsky et all., "An unidentified line in X-ray spectra of the Andromeda galaxy and Perseus galaxy cluster", Phys. Rev. Lett. 113, 251301 (2014) [arXiv: 1402.4119]

[47] A. Boyarsky et all., "Checking the dark matter origin of 3.53 keV line with the Milky Way center", Phys. Rev. Lett. 115, 161301 (2015) [arXiv: 1408.2503]

[48] T. Jeltema1 and S.Profumo, "Deep XMM Observations of Draco rule out at the 99% Confidence Level a Dark Matter Decay Origin for the 3.5 keV Line", 2015 [arXiv: 1512.01239]

[49] D. Wu, "A Brief Introduction to the Strong CP Problem", Superconducting Super Collider Laboratory, 1991

[50] R.D. Peccei, H.R. Quinn, "CP Conservation in the Presence of Pseudoparticles", Phys. Rev. Lett. 38, 1440, 1977

[51] P.W. Graham et all., "Experimental Searches for the Axion and Axion-like Particles", Annual Review if Nuclear and Particle Science 65, 2015 [arXiv: 1602.00039]

[52] CAST collaboration, "New CAST limit on the axion-photon interaction", Nature Physics 13, pp. 584-590 (2017)

[53] B. Penning, "The Pursuit of Dark Matter at Colliders - An Overview", 2017 [arXiv: 1712.01391]

[54] M. Schumann, "Direct Detection of WIMP Dark Matter: Concepts and Status", J. Phys. G46 (2019) no.10, 103003 [arXiv: 1903.03026]

[55] S.C. Martin et all., "The RAVE survey: constraining the local Galactic escape speed", Mon.Not.Roy.Astron.Soc.379:755-772, 2007

[56] K. Freese, M. Lisanti, C. Savage, "Annual Modulation of Dark Matter: A Review", [arXiv: 1209.3339v3]

[57] T.M. Undagoitia and L. Rauch, "Dark matter direct-detection experiments", J. Phys. G43 (2016) no.1, 013001 [arXiv: 1509.08767]

[58] R. Bernabei et all., "First results from DAMA/LIBRA and the combined results with DAMA/NaI", Eur.Phys.J.C56:333-355, 2008 [arXiv: 0804.2741]

[59] J.M. Gaskins, "A review of indirect searches for particle dark matter", Contemporary Physics, 2016 [arXiv: 1604.00014]

[60] F.S. Queiroz, "Dark Matter Overview: Collider, Direct and Indirect Detection Searches", Max-Planck Institute of Physics

[61] LAT collaboration, "Constraints on Dark Matter Annihilation in Clusters of Galaxies with the Fermi Large Area Telescope", JCAP 05(2010)025 [arXiv: 1002.2239]

[62] A.A. Moiseev et all., "Dark Matter Search Perspectives with GAMMA-400", 2013 [arXiv: 1307.2345]

[63] L. Covi et all., "Neutrino Signals from Dark Matter Decay", JCAP 1004:017, 2010 [arXiv: 0912.3521]

[64] B. Lu and H. Zong, "Limits on the Dark Matter from AMS-02 antiproton and positron fraction data", Phys. Rev. D 93, 103517 (2016) [arXiv: 1510.04032]

[65] J. Abdallah et all., "Simplified Models for Dark Matter Searches at the LHC", Phys. Dark Univ. 9-10 (2015) 8-23 [arXiv: 1506.03116]

[66] H. An, L. Wang, H. Zhang, "Dark matter with t-channel mediator: a simple step beyond contact interaction", Phys. Rev. D 89, 115014 (2014) [arXiv: 1308.0592]

[67] ATLAS Collaboration, "Search for dark matter and other new phenomena in events with an energetic jet and large missing transverse momentum using the ATLAS detector", JHEP 01 (2018) 126 [arXiv: 1711.03301]

[68] CMS Collaboration, "Search for new physics in the monophoton final state in proton-proton collisions at $\sqrt{s} = 13$ TeV", J. High Energy Phys. 10 (2017) 073 [arXiv: 1706.03794]

[69] CMS Collaboration, "Search for dark matter produced with an energetic jet or a hadronically decaying W or Z boson at $\sqrt{s} = 13$ TeV", JHEP 07 (2017) 014 [arXiv: 1703.01651]

[70] CMS Collaboration, "Search for new physics in final states with an energetic jet or a hadronically decaying W or Z boson and transverse momentum imbalance at $\sqrt{s} = 13$ TeV", Phys. Rev. D 97, 092005 (2018) [arXiv: 1712.02345]

[71] ATLAS Collaboration, "Search for dark matter in association with a Higgs boson decaying to two photons at $\sqrt{s} = 13$ TeV with the ATLAS detector", Phys. Rev. D 96 (2017) 112004 [arXiv: 1706.03948]

[72] CMS Collaboration, "Search for associated production of dark matter with a Higgs boson decaying to $b\bar{b}$ or $\gamma\gamma$ at $\sqrt{s} = 13$ TeV", JHEP 10 (2017) 180 [arXiv: 1703.05236]

[73] Atlas Collaboration, "Search for new phenomena in dijet events using 37 $fb^{?1}$ of pp collision data collected at $\sqrt{s} = 13$ TeV with the ATLAS detector", Phys. Rev. D 96, 052004 (2017) [arXiv: 1703.09127]

[74] CMS Collaboration, "Search for narrow and broad dijet resonances in proton-proton collisions at $\sqrt{s} = 13$ TeV and constraints on dark matter mediators and other new particles", JHEP 08 (2018) 130 [arXiv: 1806.00843]

[75] C. Munoz, "Models of Supersymmetry for Dark Matter", FTUAM 17/2, IFT-UAM/CSIC-17-005, 2017 [arXiv: 1701.05259]

[76] CMS Collaboration, "Searches for invisible decays of the Higgs boson in pp collisions at $sqrts =$ 7, 8, and 13 TeV", JHEP 02 (2017) 135 [arXiv: 1610.09218]

[77] J. Alimena et all., "Searching for long-lived particles beyond the Standard Model at the Large Hadron Collider", 2019 [arXiv: 1903.04497]

[78] A. Albert et all., "Recommendations of the LHC Dark Matter Working Group: Comparing LHC searches for heavy mediators of dark matter production in visible and invisible decay channels", 2017 [arXiv: 1703.05703]

[79] M. Tanabashi et al., Particle Data Group, Phys. Rev. D98, 030001 (2018)

[80] R. Schicker, "The ALICE detector at LHC", 2005

[81] LHCb Collaboration, "LHCb Detector Performance", Int. J. Mod. Phys. A 30, 1530022 (2015) [arXiv: 1412.6352]

[82] J.T. Boyd, "LHC Run-2 and Future Prospects", 2020

[83] E. Gschwendtner, "AWAKE, A Particle-driven Plasma Wakefield Acceleration Experiment", CERN Yellow Report CERN 2016-001, pp.271-288 [arXiv: 1705.10573]

[84] M. Thomson, "Modern Particle Physics", Cambridge University Press, 2013

[85] G. Apollinari et all., "High Luminosity Large Hadron Collider HL-LHC", CERN Yellow Report CERN-2015-005, pp.1-19 [arXiv: 1705.08830]

[86] CMS Collaboration, "The CMS experiment at the CERN LHC", JINST 3 (2008) S08004

[87] CMS Collaboration, "Precision measurement of the structure of the CMS inner tracking system using nuclear interactions", JINST 13 (2018) P10034 [arXiv: 1807.03289]

[88] M.S. Kim, "CMS reconstruction improvement for the muon tracking by the RPC chambers", 2013 JINST 8 T03001 [arXiv: 1209.2646]

[89] CMS Collaboration, "Performance of the CMS muon detector and muon reconstruction with proton-proton collisions at $\sqrt{s} = 13$ TeV", JINST 13 (2018) P06015 [arXiv: 1804.04528]

[90] CMS Collaboration, "Particle-Flow Event Reconstruction in CMS and Performance for Jets, Taus, and MET", CMS-PAS-PFT-09-001, 2009

[91] CMS Collaboration, "Description and performance of track and primary-vertex reconstruction with the CMS tracker", JINST 9 (2014) P10009 [arXiv: 1405.6569]

[92] V. Knunz, "Measurement of Quarkonium Polarization to Probe QCD at the LHC", Springer theses, 2015

[93] CMS Collaboration, "Performance of electron reconstruction and selection with the CMS detector in proton-proton collisions at $\sqrt{s} = 8$ TeV", JINST 10 (2015) P06005 [arXiv: 1502.02701]

[94] J. Rembser, "CMS Electron and Photon Performance at 13 TeV", J. Phys. Conf. Ser. 1162 012008, 2019

[95] P.L.S. Connor, "Review of jet reconstruction algorithms", Ryan Atkin J. Phys. Conf. Ser. 645 012008, 2015

[96] CMS Collaboration, "Jet energy scale and resolution in the CMS experiment in pp collisions at 8 TeV", JINST 12 (2017) P02014 [arXiv: 1607.03663]

[97] F. Beaudette, "The CMS Particle Flow Algorithm", 2014 [arXiv: 1401.8155]

[98] CMS Collaboration, "Identification of heavy-flavour jets with the CMS detector in pp collisions at 13 TeV", JINST 13 (2018) P05011 [arXiv: 1712.07158]

[99] CMS Collaboration, "Performance of missing transverse momentum reconstruction in proton-proton collisions at $\sqrt{s} = 13$ TeV using the CMS detector", JINST 14 (2019) P07004 [arXiv: 1903.06078

[100] L. Sonnenschein, "Analytical solution of ttbar dilepton equations", Phys.Rev.D73:054015, 2016

[101] M.H. Seymour and M. Marx, "Monte Carlo Event Generators", MCnet-13-05, 2013 [arXiv:1304.6677]

[102] B. Cabouat, J.R. Gaunt and K. Ostrolenk, "A Monte-Carlo Simulation of Double Parton Scattering", JHEP11(2019)061 [arXiv: 1906.04669]

[103] R. Placakyte, "Parton Distribution Functions", 2011 [arXiv:1111.5452]

[104] J. Alwall et all., "MadGraph 5 : Going Beyond", 2011 [arXiv:1106.0522]

[105] C. Oleari, "The POWHEG-BOX", Nucl.Phys.Proc.Suppl.205-206:36-41 [arXiv:1007.3893]

[106] S. Frixione et all., "The MC@NLO 4.0 Event Generator", CERN-TH/2010-216 [arXiv: 1010.0819]

[107] B. Webber, "Parton shower Monte Carlo event generators", Scholarpedia

[108] M. Bahr et all., "Herwig++ Physics and Manual", Eur.Phys.J.C58:639-707, 2008 [arXiv: 0803.0883]

[109] T. Sjostrand, "A Brief Introduction to PYTHIA 8.1" Comput.Phys.Commun.178:852-867, 2008 [arXiv: 0710.3820]

[110] A. Karneyeu et all., "MCPLOTS: a particle physics resource based on volunteer computing", European Physical Journal C 74 (2014) [arXiv: 1306.3436]

[111] V. Lefebure and S. Banerjee, "CMS Simulation Software Using Geant4", CMS-NOTE-1999-072, 1999

[112] S. Banerjee, "Validation of Geant4 Physics Models Using Collision Data from the LHC", J. Phys.: Conf. Ser. 898 042005

[113] A. Rizzi, G. Petrucciani and M. Peruzzi, "A further reduction in CMS event data for analysis: the NANOAOD format", J. Phys.: Conf. Ser. 214 06021

[114] C.G. Lester and D.J. Summers, "Measuring masses of semi-invisibly decaying particles pair produced at hadron colliders", Phys.Lett.B463:99-103, 1999

[115] K. Bloom, "CMS software and computing for LHC Run 2", ICHEP 2016 [arXiv: 1611.03215]

[116] W. Tanenbaum, "A ROOT/IO Based Software Framework for CMS", ECONFC0303241:TUKT010, 2003

[117] CMS Collaboration, "CMS Luminosity Measurements for the 2016 Data Taking Period", CMS-PAS-LUM-17-001, 2017

[118] CMS Collaboration, "CMS Luminosity Measurements for the 2017 Data Taking Period", CMS-PAS-LUM-17-001, 2018

[119] CMS Collaboration, "CMS Luminosity Measurements for the 2018 Data Taking Period", CMS-PAS-LUM-17-001, 2019

[120] CMS Collaboration, "BRIL Work Suite"